J|A|C|S
ARTICLES
Published on Web 02/08/2003

Ultrafast Singlet Excited-State Polarization in Electronically Asymmetric Ethyne-Bridged Bis[(porphinato)zinc(II)] Complexes

Igor V. Rubtsov, Kimihiro Susumu, Grigorii I. Rubtsov, and Michael J. Therien*

Contribution from the Department of Chemistry, University of Pennsylvania, Philadelphia, Pennsylvania 19104-6323

Received September 6, 2002; E-mail: therien@a.chem.upenn.edu

Abstract: The excited-state dynamics of two conjugated bis[(porphinato)zinc(II)] (bis[PZn]) species, bis-[(5,5′-10,20-bis[3,5-bis(3,3-dimethyl-1-butyloxy)phenyl]porphinato)zinc(II)]ethyne (**DD**) and [(5,-10,20-bis-[3,5-bis(3,3-dimethyl-1-butyloxy)phenyl]porphinato)zinc(II)]-[(5′,-15′-ethynyl-10′,20′-bis(heptafluoropropyl)-porphinato)zinc(II)]ethyne (**DA**), were studied by pump-probe transient absorption spectroscopy and hole burning techniques. Both of these *meso*-to-*meso* ethyne-bridged bis[PZn] compounds display *intense* near-infrared (NIR) transient $S_1 \rightarrow S_n$ absorptions and fast relaxation of their initially prepared, electronically excited Q states. Solvational and conformational relaxation play key roles in both **DD** and **DA** ground- and excited-state dynamics; in addition to these processes that drive spectral diffusion, electronically excited **DA** manifests a 3-fold diminution of $S_1 \rightarrow S_0$ oscillator strength on a 2−20 ps time scale. Both **DD** and **DA** display ground-state and time-dependent excited-state conformational heterogeneity; hole burning experiments show that this conformational heterogeneity is reflected largely by the extent of porphyrin−porphyrin conjugation, which varies as a function of the pigment−pigment dihedral angle distribution. While spectral diffusion can be seen for both compounds, rotational dynamics driving configurational averaging ($\tau \approx 30$ ps), along with a small solvational contribution, account for essentially all of the spectral changes observed for electronically excited **DD**. For **DA**, supplementary relaxation processes play key roles in the excited-state dynamics. Two fast solvational components (0.27 and 1.7 ps) increase the **DA** excited-state dipole moment and reduce concomitantly the corresponding $S_1 \rightarrow S_0$ transition oscillator strength; these data show that these effects derive from a time-dependent change of the degree of **DA** S_1-state polarization, which is stimulated by solvation and enhanced excited-state inner-sphere structural relaxation.

Introduction

Establishing delocalized electronic states in organic and biological materials requires typically the assembly of aggregates or oligomers that feature substantial interactions between the respective building block chromophores. For example, strong pigment−pigment coupling drives the formation of the delocalized electronic states characteristic of the biological light harvesting complexes;[1−4] similarly, substantial π-orbital-mediated electronic communication plays a key role in the diffuse excited states that epitomize a wide range of electrooptic materials.[5−10]

Given the established photophysics of multipigment ensembles in biology, focused efforts have been made to design and synthesize covalently linked assemblies of porphyrins and related tetrapyrrolic chromophores. While a wide range of macrocycle-to-macrocycle linkage strategies have been implemented,[11] relatively few modes of porphyrinoid−porphyrinoid connectivity provide sufficiently strong interchromophore electronic interactions to facilitate extensive electronic delocalization.[12−34] Of these families of multipigment ensembles that feature substantial ground- and/or excited-state interchromophore electronic interactions, those that feature direct ethyne-, butadiyne-, and oligoyne-based macrocycle-to-macrocycle connectivity have evinced a wide range of particularly impressive electrooptic properties.[12−28]

In the present study, we apply femtosecond transient hole burning spectroscopy to investigate the isotropic and anisotropic excited-state dynamics of two supermolecular bis-[(porphinato)zinc(II)] (bis[PZn]) species that feature a *meso*-to-*meso* ethyne-bridged linkage motif: bis[(5,5′-10,20-bis-

(1) van Grondelle, R.; Dekker, J. P.; Gillbro, T.; Sundstrom, V. *Biochim. Biophys. Acta* **1994**, *1187*, 1−65.
(2) Fleming, G. R.; van Grondelle, R. *Curr. Opin. Struct. Biol.* **1997**, *7*, 738−748.
(3) Sundstrom, V.; Pulletits, T.; van Grondelle, R. *J. Phys. Chem. B* **1999**, *103*, 2327−2346.
(4) Kumble, R.; Howard, T. D.; Cogdell, R. J.; Hochstrasser, R. M. *J. Photochem. Photobiol., A: Chem.* **2001**, *142*, 121−126.
(5) Tour, J. M. *Chem. Rev.* **1996**, *96*, 537−553.
(6) Roncali, J. *Chem. Rev.* **1997**, *97*, 173−205.
(7) Martin, R. E.; Diederich, F. *Angew. Chem., Int. Ed.* **1999**, *38*, 1350−1377.
(8) van Mullekom, H. A. M.; Vekemans, J. A. J. M.; Havinga, E. E.; Meijer, E. W. *Mater. Sci. Eng., R* **2001**, *32*, 1−40.
(9) McGehee, M. D.; Heeger, A. J. *Adv. Mater.* **2000**, *12*, 1655−1668.
(10) Friend, R. H.; Gymer, R. W.; Holmes, A. B.; Burroughes, J. H.; Marks, R. N.; Taliani, C.; Bradley, D. D. C.; Dos Santos, D. A.; Bredas, J. L.; Logdlund, M.; Salaneck, W. R. *Nature* **1999**, *397*, 121−128.

[3,5-bis(3,3-dimethyl-1-butyloxy)phenyl]porphinato)zinc(II)]-ethyne (**DD**) and [(5,-10,20-bis[3,5-bis(3,3-dimethyl-1-butyloxy)-phenyl]porphinato)zinc(II)]-[(5′,-15′-ethynyl-10′,20′-bis(hepta-fluoropropyl)porphinato)zinc(II)]ethyne (**DA**) over subpico-second through nanosecond time scales. These experiments delineate a number of special spectroscopic properties of these species that include the presence of extraordinarily intense, low energy excited-singlet manifold optical transitions. Interestingly, electronic asymmetry is shown to influence significantly the nature of the observed excited-state dynamics in these compounds, driving an unusual coupling of solvent-induced excited-state and supplemental structural relaxation processes that give rise to a time-dependent attenuation of the emission dipole moment.

Experimental Section

Materials. All manipulations were carried out under nitrogen prepurified by passage through an O_2 scrubbing tower (Schweizerhall R3-11 catalyst) and a drying tower (Linde 3 Å molecular sieves). Tetrahydrofuran (THF) was obtained from Fisher Scientific (HPLC grade) and distilled from K/benzoylbiphenyl under nitrogen. Syntheses and characterization data for bis[(5,5′-10,20-bis[3,5-bis(3,3-dimethyl-1-butyloxy)phenyl]porphinato)zinc(II)]ethyne (**DD**) and [(5,-10,20-bis[3,5-bis(3,3-dimethyl-1-butyloxy)phenyl]porphinato)zinc(II)]-[(5′,-15′-ethynyl-10′,20′-bis(heptafluoropropyl)porphinato)zinc(II)]ethyne (**DA**) have been reported previously.[20]

The Supporting Information includes a detailed description of the femtosecond transient absorption spectrometer and experimental conditions for the transient absorption and transient anisotropy studies. These experiments were carried out using a 2 mm path length Schlenk-style optical cell that allowed for circulation of the sample under nitrogen. Sample concentrations were adjusted to give an optical density of ~0.4 at the Q-state pump wavelength. All experiments were carried out at ambient temperature (23 ± 1 °C).

Computational Studies. The ground-state geometries of **DD** and **DA** were determined using the Hartree−Fock semiempirical AM1 method (HyperChem Software).[35] To determine the dependence of the relative heats of formation upon the porphyrin−porphyrin dihedral angle, each angle-dependent geometry optimization was performed until the local energy minimum was determined. To provide insight into the dipole moment changes that accompany electronic excitation of **DD** and **DA**, these Franck−Condon states were approximated as one-electron excitations in a restricted HF computation in which the minimum energy ground-state structure was not reoptimized.

Results and Discussion

Steady-State Absorption and Fluorescence Spectra of the DD and DA Bis[(porphinato)zinc(II)] Chromophores. Dimeric and multimeric porphyrin compounds that feature a *meso*-to-*meso* ethyne-bridged linkage topology manifest low energy excited states that are polarized exclusively along the long axis of the supermolecule.[12,15,16,36] The lowest energy optical transitions of these species gain in intensity and shift progressively to the red with increasing numbers of conjugated porphyrin units; notably these oligomeric compounds manifest $S_0 \rightarrow S_1$ and $S_1 \rightarrow S_0$ transition moments that are unusually enhanced with respect to those of their monomeric precursors.[12−20,36] Ambient-temperature condensed-phase structural heterogeneity in these species derives primarily from the torsional angle (θ) distribution between the respective macrocycle least-squares planes.[13,15,16] This conformational heterogeneity is manifest in the optical spectra of these species, with the lowest energy component of *x*-polarized Q-state absorption envelope corresponding to transitions emanating from maximally conjugated structures in which the torsional angles between the component porphyrin units are small; higher energy components of the Q_x band have either a vibronic genesis or derive from electron excitations of conformeric populations possessing larger torsional angles.[13,15,16]

Compound **DD** is a highly soluble analogue of previously studied examples of the *meso*-to-*meso* ethyne-bridged bis-

(11) (a) Selensky, R.; Holten, D.; Windsor, M. W.; Paine, J. B., III; Dolphin, D. *Chem. Phys.* **1981**, *60*, 33−46. (b) Davila, J.; Harriman, A.; Milgrom, L. R. *Chem. Phys. Lett.* **1987**, *136*, 427−430. (c) Osuka, A.; Kobayashi, F.; Maruyama, K. *Bull. Chem. Soc. Jpn.* **1991**, *64*, 1213−1225. (d) Biemans, H. A. M.; Rowan, A. E.; Verhoeven, A.; Vanoppen, P.; Latterini, L.; Foekema, J.; Schenning, A. P. H. J.; Meijer, E. W.; de Schryver, F. C.; Nolte, R. J. M. *J. Am. Chem. Soc.* **1998**, *120*, 11054−11060. (e) Chang, C. K.; Abdalmuhdi, I. *J. Org. Chem.* **1983**, *48*, 5388−5390. (f) Heiler, D.; McLendon, G.; Rogalskyj, P. *J. Am. Chem. Soc.* **1987**, *109*, 604−606. (g) Osuka, A.; Maruyama, K. *J. Am. Chem. Soc.* **1988**, *110*, 4454−4456. (h) Nagata, T.; Osuka, A.; Maruyama, K. *J. Am. Chem. Soc.* **1990**, *112*, 3054−3059. (i) Sessler, J. L.; Johnson, M. R.; Creager, S. E.; Fettinger, J. C.; Ibers, J. A. *J. Am. Chem. Soc.* **1990**, *112*, 9310−9329. (j) Osuka, A.; Nakajima, S.; Nagata, T.; Maruyama, K.; Toriumi, K. *Angew. Chem., Int. Ed. Engl.* **1991**, *30*, 582−584. (k) Sessler, J. L.; Capuano, V. L.; Harriman, A. *J. Am. Chem. Soc.* **1993**, *115*, 4618−4628. (l) Sugiura, K.; Tanaka, H.; Matsumoto, T.; Kawai, T.; Sakata, Y. *Chem. Lett.* **1999**, 1193−1194. (m) Vicente, M. G. H.; Smith, K. M. *J. Org. Chem.* **1991**, *56*, 4407−4418. (n) Ponomarev, G. V.; Borovkov, V. V.; Sugiura, K.; Sakata, Y.; Shul'ga, A. M. *Tetrahedron Lett.* **1993**, *34*, 2153−2156. (o) Arnold, D. P.; Borovkov, V. V.; Ponomarev, G. V. *Chem. Lett.* **1996**, 485−486. (p) Officer, D. L.; Burrell, A. K.; Reid, D. C. W. *Chem. Commun.* **1996**, 1657−1658. (q) Higuchi, H.; Shinbo, M.; Usuki, M.; Takeuchi, M.; Hasegawa, Y.; Tani, K.; Ojima, J. *Bull. Chem. Soc. Jpn.* **1999**, *72*, 1887−1898. (r) Susumu, K.; Shimidzu, T.; Tanaka, K.; Segawa, H. *Tetrahedron Lett.* **1996**, *37*, 8399−8402. (s) Osuka, A.; Shimidzu, H. *Angew. Chem., Int. Ed. Engl.* **1997**, *36*, 135−137. (t) Khoury, R. G.; Jaquinod, L.; Smith, K. M. *Chem. Commun.* **1997**, 1057−1058. (u) Prathapan, S.; Johnson, T. E.; Lindsey, J. S. *J. Am. Chem. Soc.* **1993**, *115*, 7519−7520. (v) Wagner, R. W.; Lindsey, J. S.; Seth, J.; Palaniappan, V.; Bocian, D. F. *J. Am. Chem. Soc.* **1996**, *118*, 3996−3997. (w) Strachan, J.-P.; Gentemann, S.; Seth, J.; Kalsbeck, W. A.; Lindsey, J. S.; Holten, D.; Bocian, D. F. *J. Am. Chem. Soc.* **1997**, *119*, 11191−11201. (x) Li, J.; Ambroise, A.; Yang, S. I.; Diers, J. R.; Seth, J.; Wack, C. R.; Bocian, D. F.; Holten, D.; Lindsey, J. S. *J. Am. Chem. Soc.* **1999**, *121*, 8927−8940.

(12) Lin, V. S.-Y.; DiMagno, S. G.; Therien, M. J. *Science* **1994**, *264*, 1105−1111.

(13) Lin, V. S.-Y.; Therien, M. J. *Chem.—Eur. J.* **1995**, *1*, 645−651.

(14) Angiolillo, P. J.; Lin, V. S.-Y.; Vanderkooi, J. M.; Therien, M. J. *J. Am. Chem. Soc.* **1995**, *117*, 12514−12527.

(15) Kumble, R.; Palese, S.; Lin, V. S.-Y.; Therien, M. J.; Hochstrasser, R. M. *J. Am. Chem. Soc.* **1998**, *120*, 11489−11498.

(16) Shediac, R.; Gray, M. H. B.; Uyeda, H. T.; Johnson, R. C.; Hupp, J. T.; Angiolillo, P. J.; Therien, M. J. *J. Am. Chem. Soc.* **2000**, *122*, 7017−7033.

(17) Fletcher, J. T.; Therien, M. J. *J. Am. Chem. Soc.* **2000**, *122*, 12393−12394.

(18) Fletcher, J. T.; Therien, M. J. *J. Am. Chem. Soc.* **2002**, *124*, 4298−4311.

(19) Fletcher, J. T.; Therien, M. J. *Inorg. Chem.* **2002**, *41*, 331−341.

(20) Susumu, K.; Therien, M. J. *J. Am. Chem. Soc.* **2002**, *124*, 8550−8552.

(21) Anderson, H. L. *Inorg. Chem.* **1994**, *33*, 972−981.

(22) O'Keefe, G. E.; Denton, G. J.; Harvey, E. J.; Phillips, R. T.; Friend, R. H.; Anderson, H. L. *J. Chem. Phys.* **1996**, *104*, 805−811.

(23) Beljonne, D.; O'Keefe, G. E.; Hammer, P. J.; Friend, R. H.; Anderson, H. L.; Bredas, J. L. *J. Chem. Phys.* **1997**, *106*, 9439−9460.

(24) Qureshi, F. M.; Martin, S. J.; Long, X.; Bradley, D. D. C.; Henari, F. Z.; Blau, W. J.; Smith, E. C.; Wang, C. H.; Kar, A. K.; Anderson, H. L. *Chem. Phys.* **1998**, *231*, 87−94.

(25) Kuebler, S. M.; Denning, R. G.; Anderson, H. L. *J. Am. Chem. Soc.* **2000**, *122*, 339−347.

(26) Screen, T. E.; Thorne, J. R. G.; Denning, R. G.; Bucknall, D. G.; Anderson, H. L. *J. Am. Chem. Soc.* **2002**, *124*, 9712−9713.

(27) Arnold, D. P.; Heath, G. A. *J. Am. Chem. Soc.* **1993**, *115*, 12197−12198.

(28) Arnold, D. P.; Heath, G. A.; James, D. A. *J. Porphyrins Phthalocyanines* **1999**, *3*, 5−31.

(29) Jiang, B.; Yang, S.-W.; Barbini, D. C.; Jones, W. E., Jr. *Chem. Commun.* **1998**, 213−214.

(30) Shultz, D. A.; Hyoyoung, L.; Kumar, R. K.; Gwaltney, K. P. *J. Org. Chem.* **1999**, *64*, 9124−9136.

(31) Crossley, M.; Govenlock, L. J.; Prashar, J. K. *J. Chem. Soc., Chem. Commun.* **1995**, 2379−2380.

(32) Wytko, J.; Berl, V.; McLaughlin, M.; Tykwinski, R. R.; Schreiber, M.; Diederich, F.; Boudon, C.; Gisselbrecht, J.-P.; Gross, M. *Helv. Chim. Acta* **1998**, *81*, 1964−1977.

(33) Paolesse, R.; Jaquinod, L.; Sala, F. D.; Nurco, D. J.; Prodi, L.; Lugli, P.; Smith, K. M. *J. Am. Chem. Soc.* **2000**, *122*, 11295−11302.

(34) Tsuda, A.; Osuka, A. *Science* **2001**, *293*, 79−82.

(35) Dewar, M. J. S.; Zoebisch, E. G.; Healy, E. F.; Stewart, J. J. P. *J. Am. Chem. Soc.* **1985**, *107*, 3902−3909.

(36) Uyeda, H. T.; Lin, V. S.-Y.; Williams, S. A.; Troxler, T.; Therien, M. J. Manuscript in preparation.

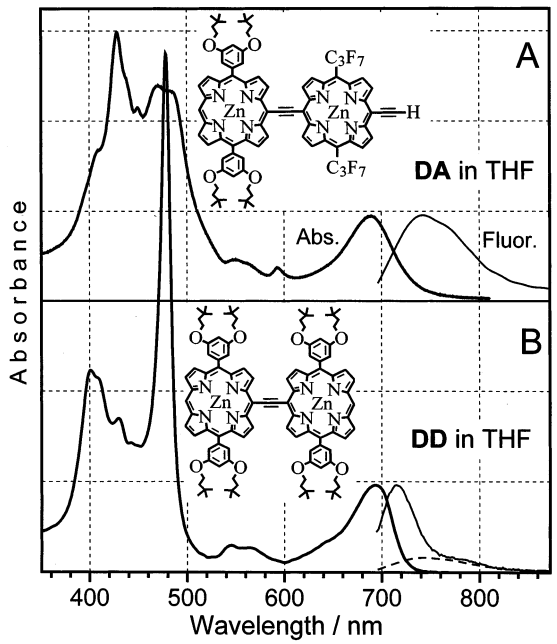

Figure 1. Normalized absorption and fluorescence spectra of (A) **DA** and (B) **DD** in THF solvent. These fluorescence spectra were obtained with an excitation wavelength of 678 nm. The dashed line in part B shows the relative fluorescence intensity of **DA** with respect to **DD** under identical excitation conditions and equivalent optical density. The maximum extinction coefficients are 317 000 $(M\ cm)^{-1}$ for **DD** in THF at 479 nm and 110 600 $(M\ cm)^{-1}$ for **DA** in THF at 429 nm.

[(porphinato)zinc(II)] (bis[PZn]) structural motif which featured simple 10,20-diaryl substituents.[12−16,20] While the optical spectroscopic features of this class of compounds have been discussed extensively,[12−16,19,20] it is worth noting that the full width at half-maximum (fwhm) **DD**'s Q_x absorption band is relatively narrow (1085 cm^{-1}) (Figure 1B), with a corresponding mirror-image fluorescence spectrum (**DD** $\lambda_{em}(max) = 711$ nm) that evinces similar Franck−Condon (FC) and relaxed excited states of the molecule.[20] The fwhm of the **DD** fluorescence band (850 cm^{-1}) is diminished slightly with respect to that of the Q_x absorption; provided that differential solvation of the ground and excited states is not extensive, these data suggest that there exists a smaller distribution of conformers in the relaxed **DD** S_1-excited state with respect to the ground state. In contrast, the **DA** Q_x band is significantly broader than that manifest by **DD** (1390 vs 1085 cm^{-1}) (Figure 1). Note also that the Q_x band in the **DA** spectrum extends further to the red relative to the analogous **DD** transition, suggesting that (i) the **DA** distribution of ground-state conformers is broader than in **DD**, (ii) the dependence of conformeric population upon the inter-ring torsional coordinate in these species differs significantly, (iii) a CT transition exists within the Q-state manifold, or (iv) the Q_x absorption oscillator strength of the most planar **DA** conformers, in contrast to the case for **DD**, is smaller than that expressed by conformers featuring larger torsional angles between their respective PZn least-squares planes (vide infra). As the **DA** molecule consists of electronically asymmetric porphyrin units, more significant outer-sphere solvent reorganization likely accompanies relaxation of the initially prepared singlet excited state with respect to the analogous **DD** state. Consistent with this notion, the **DA** Stokes shift is large (1148 cm^{-1}) relative to that evinced in the corresponding **DD** spectra (324 cm^{-1}); furthermore, the **DA** steady-state fluorescence spectrum (**DA**: $\lambda_{em}(max) = 756$ nm;[20] Figure 1A) is broad (fwhm ≈ 2170 cm^{-1}) and shows additional structure relative to the **DD** fluorescence emission (fwhm = 810 cm^{-1}).

The magnitude of the **DD** Stokes shift is consistent with the ground- and excited-state electronic structural properties of *meso*-to-*meso* ethyne-bridged bis[PZn] compounds[12−16,20] and previously published optical data for a related structure featuring unelaborated 10,20-phenyl rings.[12,13] Because of its symmetrical nature, the bis[PZn] species **DD** does not possess a ground-state dipole moment; theoretical and Stark spectroscopic studies evince however that the polarizable singlet excited states of *meso*-to-*meso* ethyne-bridged bis[PZn] compounds exhibit measurable dipolar character, with B- and Q-state $\Delta\mu_{ge}$ values determined experimentally to be on the order of ∼2 D.[16]

Meso-to-*meso* ethyne-bridged **DA**, however, possesses significant ground-state electronic asymmetry. Note that the **A** porphyrin unit of this species features macrocycle 10,20-bis-(perfluoroalkyl) groups. Potentiometric and electronic structural studies establish that [5,15-di(perfluoroalkyl)porphinato]zinc(II) species possess HOMOs and LUMOs that are uniformly lowered in energy by ∼0.3 eV relative to those of corresponding *meso*-phenyl-substituted structures.[20,37−39] The presence of non-π-conjugating, σ-electron-withdrawing perfluoroalkyl groups stabilizes extensively the PZn a_{2u} orbital; in contrast to the **D** porphyrin fragment, which possesses an a_{2u}-derived HOMO, an isolated **A** PZn species manifests an a_{1u}-symmetric highest-lying filled state.[20,37−39] Congruent with this electronic structural perturbation, semiempirical calculations suggest that **DA** manifests a ground-state dipole moment of ∼2 D (data not shown). Given such electronic features, relative to **DD**, **DA** is expected to undergo augmented excited-state structural and inner-solvation shell relaxation processes, consistent with the observed magnitude of its Stokes shift.

DD and DA Ultrafast Transient Absorption Spectra. Conventional (porphinato)zinc excited-state dynamics and spectroscopy evince fast $S_2 \rightarrow S_1$ internal conversion (<1 ps),[15] nanosecond fluorescence lifetimes, prominent excited-state absorption bands in the 400−650 nm spectral domain, and small Stokes shifts in virtually all solvents; this latter point reflects the minimal solvational and inner-sphere relaxation dynamics that accompany electronic excitation in these species. For the conjugated **DD** and **DA** compounds, inter-ring dynamics and augmented electronic structural reorganization that lead to enhanced excited-state polarization complicate this simple picture.

The fs and ps time scale transient spectra obtained for **DD** and **DA** (Figure 2 and Supporting Information) display four pronounced signatures: (i) a high oscillator strength bleach in the Soret ($S_0 \rightarrow S_2$) band region, (ii) a transient absorption between the Soret and *x*-polarized Q states in the ∼500−650 nm spectral domain, (iii) a bleach in the Q-band region that partly overlaps with the stimulated emission signal, and (iv) an *intense* near-infrared (NIR) transient $S_1 \rightarrow S_n$ (S_n = a higher lying delocalized singlet excited state) absorption [λ_{max}, **DD**($S_1 \rightarrow S_n$)

(37) DiMagno, S. G.; Williams, R. A.; Therien, M. J. *J. Org. Chem.* **1994**, *59*, 6943−6948.
(38) Goll, J. G.; Moore, K. T.; Ghosh, A.; Therien, M. J. *J. Am. Chem. Soc.* **1996**, *118*, 8344−8354.
(39) Moore, K. T.; Fletcher, J. T.; Therien, M. J. *J. Am. Chem. Soc.* **1999**, *121*, 5196−5209.

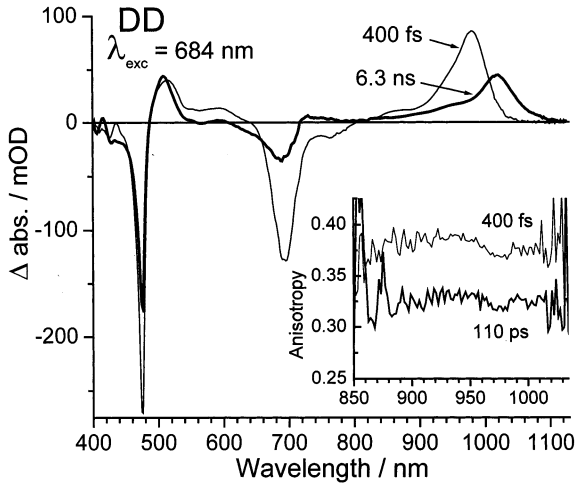

Figure 2. Transient absorption spectra of **DD** measured at delay times of 400 fs and 6.3 ns. The insets show the anisotropy of NIR transient absorptions at delay times of 400 fs and 110 ps. The excitation wavelength was 684 nm.

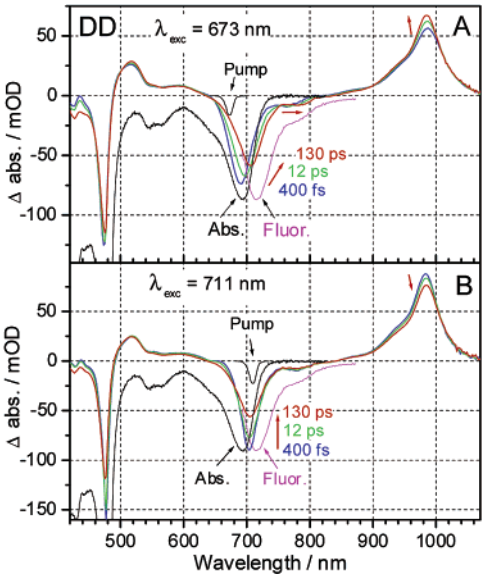

Figure 3. **DD** transient absorption spectra determined at magic angle polarization; delay times = 0.4, 12, and 130 ps: (A) $\lambda_{ex} = 673$ nm and (B) $\lambda_{ex} = 711$ nm. Normalized steady-state absorption and fluorescence spectra, as well as that of the excitation pulse, are shown inverted and displayed for comparative purposes. Thick arrows denote spectral changes that occur with increasing time.

≈ 985 nm; λ_{max}, **DA**($S_1 \rightarrow S_n$) ≈ 950 nm; see Figure 2 and Supporting Information). While the first three transient spectral features are common for porphyryl-containing compounds, strong $S_1 \rightarrow S_n$ NIR absorptions are not.

A. NIR Absorption Bands. The transient optical properties of multimeric ensembles of porphyrins and related pigments have been studied extensively. Ensembles that feature relatively weak coupling between macrocycle centers evince $S_1 \rightarrow S_n$ transitions resembling those of simple monomers; multiporphyrin aggregates, as well as cofacial porphyrin assemblies, feature transitions in the NIR, but these absorptions are $T_1 \rightarrow T_n$ in nature.[40−42] In this regard, it is worth noting that an $S_1 \rightarrow S_n$ NIR transition was predicted theoretically for a structurally related *meso*-to-*meso* butadiyne-linked bis[(porphinato)zinc(II)] compound on the basis of INDO/SCI computations,[23] but the transient optical spectroscopy of this butadiyne-bridged bis-[(octa-β-alkylporphinato)zinc(II)] complex evinced only a $T_1 \rightarrow T_n$ NIR absorption.[22] The intense $S_1 \rightarrow S_n$ NIR absorptions displayed in Figures 2 and 3 define the first examples of such excited singlet manifold transitions observed in oligomeric conjugated macrocyclic systems and highlight a potentially important spectroscopic hallmark of this class of strongly coupled porphyrin arrays (vide infra).

Polarized pump-probe spectroscopy shows that the **DD** and **DA** NIR transient absorption bands exhibit anisotropy values of 0.4 (Figure 2 and Supporting Information) when optical excitation is carried out on the red side of the respective **DD** and **DA** *x*-polarized Q-band maxima, indicating that these $S_0 \rightarrow S_1$ and $S_1 \rightarrow S_n$ transitions are mutually parallel and directed along the highly conjugated axis defined by the ethyne moiety. Interestingly, the absorption wavelength maxima of the **DD** and **DA** $S_1 \rightarrow S_n$ transitions (**DD**: ∼985 nm, 1.26 eV; **DA**: ∼950 nm, 1.30 eV) indicate that the energies of the corresponding $S_0 \rightarrow S_n$ absorptions are ∼3.1 eV; as this energy (∼400 nm) lies slightly to the blue of the high oscillator strength *x*-polarized B-state absorptive manifold,[12−20] $S_1 \rightarrow S_n$ electronic excitation likely populates either directly the S_2 level or a close-lying singlet state that can relax to a B-state within the ultrafast time domain.

B. Triplet−Triplet Transitions. The signals observed at a time delay of 6.3 ns (Figure 2 and Supporting Information) correspond to the triplet-state transient absorption spectra. In addition to the expected spectral features in the B and Q spectral regions,[14,16] strong NIR $T_1 \rightarrow T_n$ absorption bands are observed for both the **DD** and **DA** compounds. These NIR $T_1 \rightarrow T_n$ transient signals bear features in common with that elucidated for a nonfluorescent *meso*-to-*meso* butadiyne-bridged bis[(octa-β-alkylporphinato)zinc(II)] complex,[22] though the absorption in the **DD** compound is both more intense and more red shifted. Interestingly, the entire transient spectrum observed at a 6.3 ns delay for **DA** (Supporting Information) exhibits significantly diminished relative intensity with respect to that obtained for **DD**, consistent with disparate excited-state dynamics in these two *meso*-to-*meso* ethyne-bridged bis(PZn) complexes (vide infra).

The spectral changes following electronic excitation that are associated with the Soret band region are small relative to that observed at lower energy; note that the Soret spectral bleaching signature evolves little with time and is consistent with a first-order B-state electronic structural description for these species in which excitonic interactions drive primarily the mixing of PZn electronic states.[12,13,15] As the delocalized states associated with the *x*-polarized Q and the NIR $S_1 \rightarrow S_n$ transitions exhibit the most significant relaxation dynamics, we focus our analysis on the transient signals in these low energy spectral windows.

DD Spectral Hole Burning Experiments. A. Q-band Dynamics. Because of ground-state conformational heterogeneity, a spectrally narrow Q_x-state excitation pulse burns a hole

(40) Siggel, U.; Bindig, U.; Endisch, C.; Komatsu, T.; Tsuchida, E.; Voigt, J.; Fuhrhop, J.-H. *Ber. Bunsen-Ges. Phys. Chem.* **1996**, *100*, 2070−2075.
(41) Bilsel, O.; Rodriguez, J.; Milam, S. N.; Gorlin, P. A.; Girolami, G. S.; Suslick, K. S.; Holten, D. *J. Am. Chem. Soc.* **1992**, *114*, 6528−6538.
(42) Bilsel, O.; Milam, S. N.; Girolami, G. S.; Suslick, K. S.; Holten, D. *J. Phys. Chem.* **1993**, *97*, 7216−7220.

within the conformeric distribution; spectral diffusion in both the ground and excited states thus plays a key role in the time-dependent evolution of the transient spectrum. Optical pumping on the blue side of the **DD** Q_x manifold ($\lambda_{ex} = 673$ nm; Figure 3A) excites distribution ground-state conformers that feature a relatively large torsional angle (θ) distribution between the respective macrocycle least-squares planes. The Q-band region (650−750 nm) transient bleach red shifts with increasing time; these fast dynamics are finished within ∼100 ps. Note that the **DD** transient spectra obtained at the $t = 130$ ps delay for both blue ($\lambda_{ex} = 673$ nm) and red ($\lambda_{ex} = 711$ nm) Q_x manifold excitations are identical (Figure 3A, B).

In a case where the excited-state conformeric torsional angular distribution is similar to that of the ground state, excitation on the blue side of the **DD** Q_x manifold initiates spectral diffusion in the ground state toward structures having larger interporphyryl torsional angles θ, while excited-state spectral diffusion gives rise to a distribution of structures featuring a smaller average torsional angle θ between the macrocycle least-squares planes. Such relaxation (equilibration) processes would result in a red shift of both the ground-state bleach and stimulated emission signals in the fast time domain ($t < 100$ ps). Moreover, as the **DD** conformers having smaller torsional angles θ would possess larger transition moments, the bleach and stimulated emission spectral signals would be expected to increase in amplitude. While the red shift of the Q-band transient spectrum is observed as expected (Figure 3A), there is a decrease of the amplitude of the transients over the 0.4-to-100 ps time domain (opposite to the expectation), suggesting the existence of another excited-state relaxation process.

Excitation on the red side of the **DD** Q_x manifold ($\lambda_{ex} = 711$ nm) gives rise to different early time dynamics (Figure 3B). Note that there is no energy shift of the bleach minimum at 705 nm; this spectral feature only decreases in intensity and broadens (33%) with time. As a 711 nm pulse would be expected to excite distribution ground-state conformers that feature a smaller average interporphyryl torsional angle with respect to 673 nm excitation,[15] spectral diffusion occurs in the ground state toward structures having smaller interporphyryl torsional angles θ, while excited-state spectral diffusion gives rise to a distribution of structures featuring a larger average torsional angle θ between the macrocycle least-squares planes. Provided gross differences do not exist between the ground- and excited-state torsional angle distributions; such equilibration processes would drive blue shifts of the ground-state bleach and stimulated emission transients and decrease their respective amplitudes over the time scale of these relaxation dynamics. While there is a significant decrease of the transient spectrum amplitude with time, no blue shift is observed in the experiment (Figure 3B); these data point to the existence of an additional excited-state relaxation process which causes a red shift of the Q-band transient spectrum and decreases its amplitude.

B. Dynamic Changes in the NIR Transient Band. The NIR transient absorption band (∼985 nm) also exhibits fast dynamics; in contrast however to the Q manifold transients, this transition exhibits only a minor energy shift [$\sim \pm 20$ cm^{-1}) and amplitude changes with time. Over the 0.4-to-130 ps time domain (Figure 3A, B), when $\lambda_{ex} = 711$ nm, note that the NIR absorption decreases in intensity with time; in contrast, a time-dependent increase in absorption amplitude over these same delay times is observed when $\lambda_{ex} = 673$ nm (Figure 3A). The direction of the band maximum shift over this time window also depends on the excitation wavelength: 2 nm blue and red shifts occur, respectively, for 673 and 711 nm excitations, indicating that the NIR band has a slightly higher frequency for conformers having smaller interprophyryl torsional angles θ. These data indicate that the oscillator strength of the $S_1 \rightarrow S_n$ transition increases with increasing PZn−PZn conjugation (Figure 3A, B); the spectral behavior observed for the 985 nm transient over this time domain is in complete agreement with previously discussed expectations for S_1-state structural relaxation associated with the interporphyryl angular (θ) distribution equilibration.

C. Global Analysis. Identical characteristic relaxation times of ∼30 ps are obtained from global fitting of the NIR band transients for both excitations. All transient signals evince a slowly decaying component (1.12 ns) that corresponds to the intrinsic S_1-excited-state lifetime. The 30 ps component is thus attributed to the conformeric interconversion time between populations of structures that differ with respect to their interporphyryl torsional angles; the time constant for spectral evolution coincides with that determined earlier from single-wavelength pump-probe transient anisotropy measurements obtained for an analogous *meso*-to-*meso* ethyne-bridged bis-[P(Zn)] complex featuring unelaborated 10- and 20-phenyl rings and is consistent with its previous assignment to interporphyryl ring torsional dynamics.[15] It is interesting that the NIR band frequency appears to be relatively insensitive to the extent of interporphyryl conjugation, as seen by the modest 2 nm shift of the absorption maximum that occurs with excited-state structural equilibration (vide infra). Whatever additional relaxation process is important to the description of the Q-state dynamics thus has apparently little impact on the time-dependent behavior of the $S_1 \rightarrow S_n$ transition.

In contrast to the NIR absorption band, a global fit of the time-dependent Q-band transient bleach dynamics for 711 nm excitation (Figure 3B) evinces four relaxation processes: 270 ± 120 fs, 1.9 ± 0.5 ps, 30 ± 5 ps, and 1.12 ± 0.2 ns. While the 30 ps and 1.12 ns components correspond, respectively, to interporphyryl torsional dynamics and the intrinsic excited-state lifetime, the two ultrafast components are very close to the experimentally established THF solvent relaxation times ($\tau_1 =$ 230 fs (44.7%); $\tau_2 = 1.52$ ps (55.3%); $\tau_{average} = 0.94$ ps).[43] Congruently, an analogous fit of the transient data obtained for 673 nm excitation (Figure 3A) gives characteristic relaxation times of 250 ± 70 fs, 1.7 ± 0.5 ps, 30 ± 4 ps, and 1.12 ± 0.2 ns. The decay-associated spectra (DAS) obtained for both excitation wavelengths are shown in Figure 4. For 673 nm excitation, all three fast components cause a red shift of the spectrum (Figure 4A), because of their S-like spectral shape which displays decay on the blue side and a rise on the red side of the transient. For 711 nm excitation, the DAS of the three fast components exhibit similar shapes (Figure 4B); note, however, in contrast to the DAS of Figure 4A, these spectra are negative at the bleach minimum and positive on the blue and red sides of the Q-state transient, causing time-dependent broadening of the transient spectrum. All three fast

(43) Reynolds, L.; Gardecki, J. A.; Frankland, S. J. V.; Horng, M. L.; Maroncelli, M. *J. Phys. Chem.* **1996**, *100*, 10337−10354.

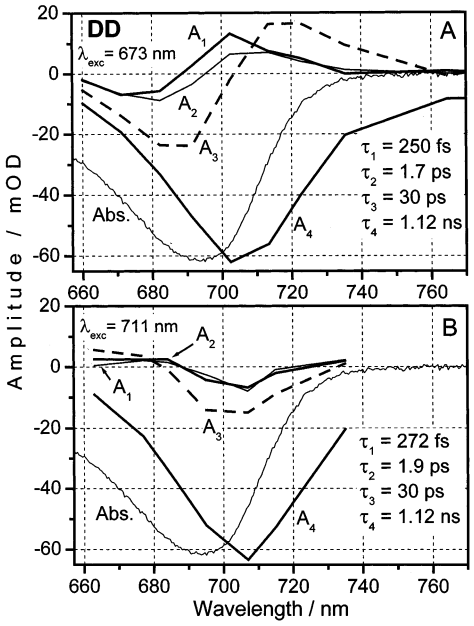

Figure 4. Decay associated spectra and corresponding time constants for **DD**: (A) λ_{ex} = 673 nm and (B) λ_{ex} = 711 nm. An inverted, normalized **DD** absorption spectrum is shown in these figures for comparison. See text for details.

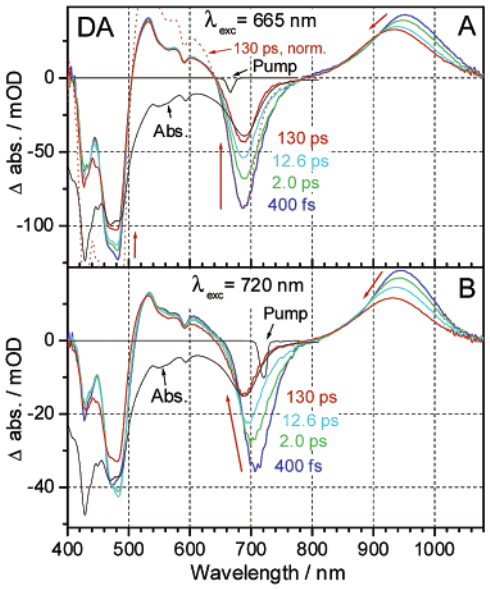

Figure 5. **DA** transient absorption spectra determined at magic angle polarization; delay times = 0.4, 2.0, 12.6, and 130 ps: (A) λ_{ex} = 665 nm and (B) λ_{ex} = 720 nm. Normalized steady-state absorption and excitation pulse spectra are inverted and displayed for comparative purposes. Thick arrows denote spectral changes that occur with increasing time. The dotted line in part A shows the spectrum recorded at the 130 ps delay normalized to match the analogous spectrum recorded at the 400 fs delay at the Q-band bleach maximum (685 nm).

components effect a decrease in the bleach band amplitude, as the amplitude of the negative part of the DAS spectrum is larger than that of the positive (Figure 4B). These features of the **DD** DAS are further discussed in the analysis of the analogous **DA** DAS later.

DA Spectral Hole Burning Experiments. A. Q-band Dynamics. Ultrafast transient spectra recorded for *meso*-to-*meso* ethyne-bridged bis[PZn] complex **DA** exhibit more pronounced time-dependent changes than were evinced in the analogous **DD** spectra (Figure 5). When **DA** is excited at 665 nm (Figure 5A), the position of the Q_x transient bleach does not shift with increasing time; in contrast, when this species is electronically excited on the red side of the absorption band (720 nm), the Q_x bleach signal shifts to the blue (Figure 5B). Similar to the dynamics observed for **DD**, evolution of the **DA** transient spectra is complete within ~100 ps of the pump pulse. In addition to the spectral features evident in Figure 5 that derive from spectral diffusion, other relaxation processes clearly play a significant role in the **DA** dynamics.

Figure 5A (λ_{ex} = 665 nm), in addition to showing that the Q_x transient bleach exhibits little time-dependent spectral shift, highlights that this signal exhibits a 2-fold decrease in amplitude and loses intensity on the low energy side of the band over the 0.4-to-100 ps time domain. This latter effect causes narrowing of the transition and is significant, since spectral diffusion alone would be expected to give either (i) a slight red shift of the band with an increase of amplitude (as was observed for 673 nm excitation of **DD**) or (ii) at least peak broadening without any shift. Note also that the shape of the relaxed Q-state transient signal ($t \approx$ 130 ps) resembles the steady-state absorption band, indicating that stimulated emission is strongly suppressed at this time delay. A similar time-dependent loss of stimulated emission intensity is evident in the Figure 5B transient spectra (λ_{ex} = 720 nm), indicating that the $S_1 \rightarrow S_0$ transition oscillator strength is significantly diminished at time delays > 100 ps. This behavior contrasts strongly the excited-state dynamics evinced for **DD**, where fast relaxation processes have little effect on the $S_1 \rightarrow S_0$ transition moment and the time-dependent contribution of stimulated emission to the transient spectra remains essentially constant.

B. Dynamic Changes in the NIR Transient Band. Significant dynamics are observed in the **DA** NIR band (~935 nm). In contrast to the analogous **DD** transient spectra, where only small amplitude changes and minor energy shifts of the $S_1 \rightarrow S_n$ transition are evident over the 0.4−130 ps time domain, the **DA** NIR band (Figure 5A, B) exhibits a time-dependent decrease in amplitude and substantial blue shift (240 cm^{-1}, λ_{ex} = 665 nm; 150 cm^{-1}, λ_{ex} = 720 nm) during the initial 100 ps following excitation. Similar to the **DD** NIR transient dynamics (Figure 3), the frequency of the **DA** NIR transition is larger for conformers having smaller interporphyryl torsional angles θ [λ_{max} ($S_1 \rightarrow S_n$) = 953 nm (λ_{ex} = 660 nm), 945 nm (λ_{ex} = 720 nm)] in the initially probed electronically excited state (0.4 ps delay). Assuming for these two excitation wavelengths that spectral diffusion shifts the NIR absorption maximum in opposite directions to the same extent (as was observed for **DD**), we find the magnitude of the blue shift caused by additional excited-states relaxation process is ~195 cm^{-1}, while the spectral diffusion contribution is ~±45 cm^{-1}.

Similar to the **DD** transient spectra, the **DA** Q-band spectral region exhibits more significant time-dependent spectral changes relative to the NIR transition. This may derive from the fact that excited-state relaxation reduces the coupling of the S_1 state to the less-delocalized ground state to a greater degree than this relaxation decouples S_1 with the delocalized, higher lying S_n excited state.

C. Global Analysis. Four exponential functions are needed to globally fit the **DA** transient dynamical data; near identical

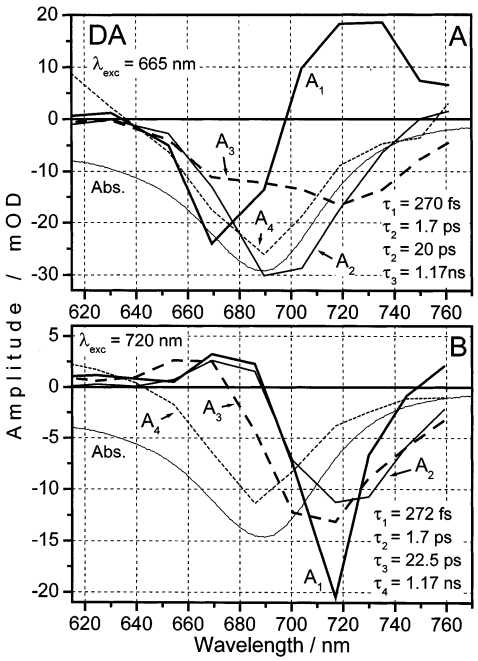

Figure 6. Decay associated spectra and corresponding time constants for **DA**: (A) λ_{ex} = 665 nm and (B) λ_{ex} = 720 nm. An inverted, normalized **DA** absorption spectrum is shown in these figures for comparison. See text for details.

characteristic times were obtained from fitting the transient data obtained at the two excitation wavelengths (for λ_{exc} = 665 nm, τ_1 = 270 ± 60 fs, τ_2 = 1.7 ± 0.4 ps, τ_3 = 20 ± 6 ps, and τ_4 = 1.17 ± 0.1 ns; for λ_{exc} = 720 nm, τ_1 = 272 ± 60 fs, τ_2 = 1.7 ± 0.3 ps, τ_3 = 22.5 ± 4 ps, and τ_4 = 1.17 ± 0.1 ns). Analogous to the characteristic relaxation times evinced for **DD**, the two fastest time constants correspond to established THF solvational dynamics.[43] The 22 ps time constant is comparable in magnitude to the evaluated time constant for torsional motion in **DD** ($\tau_3 \approx$ 30 ps). The differences in the magnitudes of these **DD** and **DA** τ_3 values likely derive from the dissimilar hydrodynamic volumes of the **D** and **A** porphyrin *meso* substituents (3,5-bis(3,3-dimethyl-1-butyloxy)phenyl in **D** vs heptafluoropropyl in **A**).[44]

The **DA** Q-state bleach region DAS for 665 nm excitation are shown in Figure 6A. The fastest component (τ_1) is negative on the blue side of the band and positive at the red side, driving a bleach band red shift. Because the fast inertial solvational component derives primarily from solvent electronic polarization, these dynamics serve to preferentially stabilize the Q state, causing a red shift of the transition. The second solvational component (τ_2 = 1.7 ps) is associated with solvent dipole reorientation, this component of the DAS peaks at the stimulated emission maximum of the nonrelaxed excited state, diminishing the stimulated emission signal. The third DAS component (τ_3 = 22 ps) shows decay throughout the entire Q-band region, displaying a maximum on the stimulated emission side of the band. The second and third DAS components thus effect emission amplitude decay rather than a spectral shift. In contrast to the analogous DAS analysis for **DD**, solvent dynamics and excited-state structural evolution in **DA** induce relaxation that decreases the $S_1 \rightarrow S_0$ transition moment. The DAS for excitation at 720 nm exhibit similar trends (Figure 6B), with the fastest inertial component causing a blue shift of the bleach band maximum and a slight increase in the spectral width and the second and third spectral decay components effecting a decrease of the stimulated emission signal and further contributing to the time-dependent blue shift of the bleach band.

The data displayed in Figures 3−6 evince the key roles played by solvational dynamics and conformational equilibration in the time-dependent inhomogeneous broadening of the **DD** and **DA** Q-state bleach signals. While the subset of molecules excited in these **DD** and **DA** hole burning experiments each possess nonequilibrium interporphyryl dihedral angle distributions and unrelaxed solvation shells, fundamental differences exist between these species regarding the nature of the dynamics associated with the fast τ_2 and τ_3 spectral decay time constants. In contrast to **DD**, these two decay components not only contribute to ground- and excited-state conformational equilibration in **DA** but also effect excited-state relaxation that causes a sharp decrease in the emission dipole moment. Given the electronically asymmetric structure of **DA**, it is likely that the observed loss of emission amplitude correlates with a time-dependent increase of excited-state polarization. Solvational processes associated with the longer time scale THF solvent relaxation (τ_2) stabilize **DA** excited states with larger dipole moments, thus decreasing the $S_1 \rightarrow S_0$ transition oscillator strength. The third fast **DA** spectral decay time (τ_3 = 22 ps), assigned to torsional dynamics about the PZn−PZn *meso*-to-*meso* ethyne bond, also effects a diminution of the $S_1 \rightarrow S_0$ emission dipole strength (Figure 6A, B). The origin of this unusual effect derives from an apparent strong coupling of solvent-induced excited-state electronic relaxation in **DA** with supplemental structural relaxation; these relaxation dynamics, which are absent in the **DD** case, serve to drive formation of an excited-state conformeric distribution having an increasingly smaller mean interporphyryl torsional angle throughout the 0.4-to-100 ps time domain. The dynamics associated with the τ_2 and τ_3 time constants thus exhibit a type of positive feedback: as the mean interporphyryl dihedral angle decreases, further solvent dipolar reorientation is possible, increasing the polarization of the S_1-state electronic wave function, which in turn makes possible augmented diminution of the PZn−PZn torsional angle and even larger excited-state electronic polarization energetically favorable. This time-dependent increase in the dipolar character of the **DA** S_1-state electronic distribution opens additional excited-state decay channels which decrease the oscillator strength of the $S_1 \rightarrow S_0$ transition relative to that observed in the **DD** case.

Spectroscopic Signatures Correlated with Equilibrated DD and DA Conformeric Distributions. The shape of the **DA** low energy *x*-polarized Q-state absorption band differs from that

(44) The evaluated structural relaxation times (for τ_3, **DD** = 30 ps and **DA** = 22 ps) can be compared to that determined for a related **DD** species, bis-[(5,5′,-10,20-diphenylporphinato)zinc(II)]ethyne (**DD′**; for τ_3, **DD′** = 30 ps), from single wavelength pump-probe transient anisotropy experiments.[15] The **DD′** PZn−PZn torsional dynamics were determined in 10:1 chloroform/pyridine.[15] While the hydrodynamic volume of the **DD′** 10- and 20-substituents is less than that expressed by **DD**, note that the solvent viscosity of 10:1 chloroform/pyridine is slightly larger than that for THF (∼0.61 vs 0.55 cP); furthermore, the hydrodynamic volume of the **DD′** PZn units is augmented because of the presence of a strongly ligating pyridine Lewis base. While it is difficult to take into account all these factors quantitatively, we conclude that the evaluated torsional dynamics for **DD**, **DA**, and **DD′** are in agreement and consistent with the expectation that hydrodynamic volume and solvent viscosity are primary determinants of the conformational mixing rate constant for this class of conjugated multiporphyrin compounds.

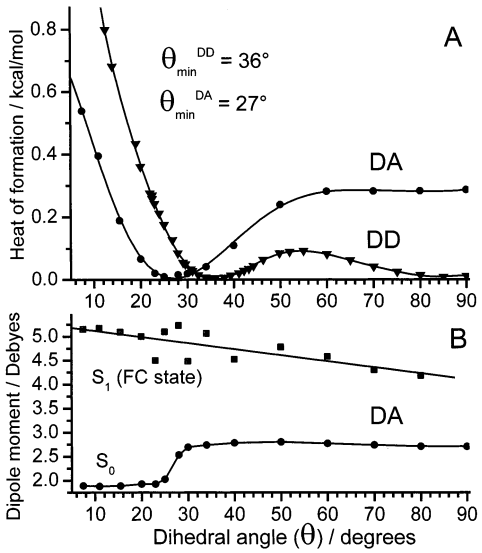

Figure 7. (A) A comparison of computed relative heats of formation determined as a function of the torsional angle between the respective (porphinato)zinc(II) least-squares planes of the **DD** and **DA** compounds. (B) Permanent dipole moments calculated for **DA** in the ground and Franck−Condon excited states as a function of the interporphyryl torsional angle. See text for computational details.

of the **DD** dimer (Figure 1). Semiempirical calculations (AM1 method) suggest that the lowest energy ground-state structure for **DA** possesses a smaller interporphyryl torsional angle than that for **DD** (Figure 7). If steric clashes between the porphyryl β hydrogens that flank the *meso*-to-*meso* ethyne bridge were absent, as in the case for analogous butadiyne-linked bis[PZn] species,[12−14] a structure in which the interporphyryl torsional angle θ corresponded to 0° would have the lowest energy. Because of increased ruffling in *meso*-perfluoroalkylporphyrin macrocycles relative to their simple phenyl-substituted analogues,[37−39,45] dihedral-angle-dependent steric interactions are reduced in **DA** relative to **DD** (Figure 7A), consistent with the computation of a **DA** minimum energy structure which possesses a torsional angle 9° less than its **DD** counterpart. These AM1 calculations predict interestingly that, at **DA** interporphyryl torsional angles less than the 27° energetic minimum, the **A** porphyrin macrocycle undergoes increasingly larger amplitude ruffling distortions; this augmented **A** ruffling that occurs concomitantly with decreasing **DA** interporphyryl dihedral angle serves to decrease the ground-state dipole moment (μ_{gg}) in this bis[PZn] compound by ∼1 D (Figure 7B). Estimation of the dipole moment associated with the S_1 Franck−Condon (FC) state (approximated as a one-electron excitation in a restricted HF computation in which the minimum energy ground-state structure was not reoptimized) suggests that μ_{ee} changes little (on the order of 1.5 D) as the interporphyryl dihedral angle decreases from 90° to 0° (Figure 7B). As a result, the dipole moment change between ground and excited FC states increases with diminishing values of the dihedral angle (Figure 7B). These calculations thus predict a dihedral-angle-dependent energetic splitting of the S_0 and S_1 potential energy surfaces and a correspondingly sensitive dependence in the FC overlap for the $S_1 \rightarrow S_0$ electronic transition. Thus, the **DA** $S_1 \rightarrow S_0$ transition moment is predicted to peak at an interporphyryl dihedral angle close to 30°; likewise, this analysis suggests that the emission dipole strength decreases (i) substantially at smaller torsional angles θ because of the increased charge transfer (CT) character of the transition and (ii) slightly at larger θ values because of diminished PZn−PZn electronic delocalization in the S_0 and S_1 states. This effect likely plays a key role in determining the shape of the low energy *x*-polarized Q absorption band, which is much more symmetrical in **DA** relative to **DD** (Figure 1); note that an analogous dihedral-angle-dependent $S_1 \rightarrow S_0$ transition moment analysis for the **DD** dimer (data not shown) shows much less variance in the extent of $S_1 \rightarrow S_0$ FC overlap, consistent with the comparatively abrupt decrease in the extinction coefficient with increasing wavelength observed on the red edge of its Q_x transition (Figure 1B).

Excitonic interactions play a prominent role in determining the conspicuous B-band ($S_0 \rightarrow S_2$) spectral features in these compounds.[12,13,15,16] As discussed previously,[12,13,15,16] the shape and energy of the *x*-polarized, sharp B-state transition is not sensitive to the PZn−PZn torsional angle distribution about the *meso*-to-*meso* ethyne bond. Consistent with this, the red shifted, *x*-polarized B-state absorption component of the **DD** and **DA** spectra does not show significant spectral diffusion dynamics (Figures 3, 5). In contrast, for the higher energy B-state absorption envelope, which features significant contributions from *y*-polarized transitions,[12,13,15,16] both the transition moment and transition frequency depend intimately on the magnitude of the torsional angle between the PZn least-squares planes; consistent with this, **DD** and **DA** manifest fast dynamics at wavelengths <450 nm (Figures 3, 5).

Solvent dynamics clearly play an important role in both **DD** and **DA** spectral evolution. While it is unusual to observe such dynamics for a symmetric chromophore such as **DD**, it is consistent with electroabsorption experiments (77 K, 2-methyl-THF glass) that evince that similar *meso*-to-*meso* ethyne-bridged bis[PZn] compounds exhibit B- and Q-state $\Delta\mu_{ge}$ values on the order of ∼2 D[16] and a variety of spectroscopic and theoretical analyses of these species and closely related compounds that indicate that their singlet excited states possess some cumulenic character.[12,13,15,16,46−50] The fast solvational dynamics observed for **DD**, coupled with the dihedral-angle-dependent $S_1 \rightarrow S_0$ transition moment analysis, are also consistent with a time-dependent change of the magnitude of $\Delta\mu_{ge}$; the analogous data obtained for electronically asymmetric **DA**, in which the **A** PZn fragment frontier orbitals (FOs) lie ∼0.3 eV lower in energy relative to their **D** PZn fragment FO counterparts,[20,37−39] indicate that the change in dipole moment between the corresponding conformationally equilibrated **DA** S_0 and S_1 states is substantially larger.

Estimation of the DD and DA Transition Moments. The ratio of the Q-state transition moments ($\xi = M^{DD}_{e\rightarrow g}/M^{DA}_{e\rightarrow g}$) for **DD** and **DA** can be estimated from the absorption and emission spectra. The Q-state transition moment ratio obtained

(45) Wertsching, A. K.; Koch, A. S.; DiMagno, S. G. *J. Am. Chem. Soc.* **2001**, *123*, 3932−3939.
(46) LeCours, S. M.; Guan, H.-W.; DiMagno, S. G.; Wang, C. H.; Therien, M. J. *J. Am. Chem. Soc.* **1996**, *118*, 1497−1503.
(47) Priyadarshy, S.; Therien, M. J.; Beratan, D. N. *J. Am. Chem. Soc.* **1996**, *118*, 1504−1510.
(48) Karki, L.; Vance, F. W.; Hupp, J. T.; LeCours, S. M.; Therien, M. J. *J. Am. Chem. Soc.* **1998**, *120*, 2606−2611.
(49) LeCours, S. M.; DiMagno, S. G.; Therien, M. J. *J. Am. Chem. Soc.* **1996**, *118*, 11854−11864.
(50) LeCours, S. M.; Phillips, C. M.; dePaula, J. C.; Therien, M. J. *J. Am. Chem. Soc.* **1997**, *119*, 12578−12589.

from electronic absorption spectral data (ξ_A) is 1.08.[20] The corresponding transition moment ratio can be calculated from the fluorescence spectrum using eq 1.[51]

$$|M|_{e\rightarrow g} = 1785.7\left[\frac{k_{rad}}{n^3 f(n)}\frac{\int F(\nu)\,d\nu}{\int F(\nu)\nu^{-3}\,d\nu}\right]^{1/2} \quad (1)$$

The ratio of transition moments ξ_{fl} is determined by eq 2−4,

$$\xi = \frac{M^{DD}_{e\rightarrow g}}{M^{DA}_{e\rightarrow g}} = \sqrt{\frac{k^{DD}_{rad}}{k^{DA}_{rad}}\frac{\tilde{\nu}^3_{DA}}{\tilde{\nu}^3_{DD}}} \quad (2)$$

$$\tilde{\nu}^3 = \frac{\int F(\nu)\nu^{-3}\,d\nu}{\int F(\nu)\,d\nu} \quad (3)$$

$$\frac{\Phi^{DD}_{fl}}{\Phi^{DA}_{fl}} = \frac{\int\frac{F_{DD}(\nu)}{\nu}\,d\nu}{\int\frac{F_{DA}(\nu)}{\nu}\,d\nu}\frac{(1-10^{-D_{DA}})}{(1-10^{-D_{DD}})} \quad (4)$$

where D_{DD} and D_{DA} are optical densities of the two samples at the excitation wavelength. The **DD**/**DA** fluorescence quantum yield ratio (eq 4) is 2.94, with the corresponding ratio of radiative rate constants equal to 3.1. The ξ_{fl} value thus equals 1.7, which is 1.6 times larger than ξ_A. If there were no electronic relaxations in the **DA** S_1 excited state, the ratio of the absorption and emission transition moments (ξ_A/ξ_{fl}) should be unity; this analysis of steady-state absorption and emission data shows that excited-state relaxation in **DA** suppresses the $S_1\rightarrow S_0$ transition moment and the consequent emission transition probability, by factors of 1.6 and 2.6, respectively.

Conclusions

Time-resolved polarized pump-probe spectroscopic studies show that the excited states of *meso*-to-*meso* ethyne-bridged bis[(porphinato)zinc(II)] compounds **DD** and **DA** display a number of unusual spectroscopic and dynamic properties. An *intense* NIR $S_1\rightarrow S_n$ absorption defines the most remarkable transient spectral feature evinced by these species; such excited-state singlet manifold transitions have thus far lacked precedent in multiporphyrin compounds. The **DD** and **DA** NIR transient absorption bands evince oscillator strengths of similar magnitude to the B-state manifold bleach (Figures 2−3, 5); equally noteworthy, the respective $S_1\rightarrow S_n$ absorption maxima of these conjugated supermolecules lie ∼3400 cm^{-1} (0.42 eV) to the red of their corresponding fluorescence emission bands, suggesting that **DD** and **DA**, as well as related structures within this class of conjugated chromophoric supermolecues,[52] can be electronically excited at energies significantly less than the $S_0\rightarrow S_1$ optical gap. Furthermore, the absorption wavelength maxima of the **DD** and **DA** $S_1\rightarrow S_n$ transitions (for **DD**, ∼985 nm, 1.26 eV; for **DA**, ∼950 nm, 1.30 eV) indicate that the energies of the corresponding $S_0\rightarrow S_n$ absorptions are ∼3.1 eV; as this energy (∼400 nm) lies slightly to the blue of the high oscillator strength *x*-polarized B-state absorptive manifold,[12−16] $S_1\rightarrow S_n$ electronic excitation likely either populates directly the S_2 level or a close-lying singlet state that can relax to a B-state within the ultrafast time domain. While these spectral properties are unusual with respect to other types of porphyrin-based multipigment structures, it is noteworthy that they bear features in common with a variety of light-emissive semiconducting polymers.[9,53−55]

DD and **DA** exhibit significant dynamics in both the Q-state and NIR spectral domains. Transient anisotropic dynamical studies establish that the respective *x*-polarized Q ($S_0\rightarrow S_1$) and NIR absorptive ($S_1\rightarrow S_n$) transitions of these species are mutually parallel and directed along the highly conjugated axis defined by the ethyne moiety. The excited-state dynamics of these species are determined by four characteristic times that correspond to the solvent inertial (τ_1) and dipolar (τ_2) relaxation, interporphyryl torsional motion (τ_3), and the intrinsic excited-state lifetime (τ_4). When these species are optically pumped on the red side of the Q_x transition, the **DD** characteristic decay times are 270 ± 120 fs, 1.9 ± 0.5 ps, 30 ± 5 ps, and 1.12 ± 0.2 ns, while the analogous **DA** dynamics evince τ_1 = 272 ± 60 fs, τ_2 = 1.7 ± 0.3 ps, τ_3 = 22.5 ± 4 ps, and τ_4 = 1.17 ± 0.1 ns.

While the subset of molecules excited in these **DD** and **DA** hole burning experiments each possess nonequilibrium interporphyryl dihedral angle distributions and unrelaxed solvation shells, key differences exist between these species regarding the nature of the dynamics associated with the fast τ_2 and τ_3 spectral decay time constants. Analyses of the decay associated spectra (DAS) obtained for **DD** and **DA** show that, in contrast to the **DD** case, these τ_2 and τ_3 decay components not only contribute to ground- and excited-state conformational equilibration in **DA** but also effect excited-state relaxation that causes a sharp decrease in the emission dipole moment. Solvational processes associated with the longer time scale THF solvent relaxation (τ_2) stabilize **DA** excited states with larger dipole moments, effecting increased excited-state polarization and a concomitant decrease in the $S_1\rightarrow S_0$ transition oscillator strength. Interporphyryl ring torsional dynamics (τ_3 = 22 ps) serve to augment the extent of (porphinato)zinc(II)−(porphinato)zinc(II) (PZn−PZn) conjugation in **DA** and thereby increase the magnitude of charge resonance interactions in the electronically asymmetric supermolecular chromophore. This strong coupling of solvent-induced excited-state electronic relaxation in **DA** with supplemental structural relaxation, which is absent in the **DD** case, not only drives formation of an excited-state conformeric distribution having an increasingly smaller mean interporphyryl torsional angle over the 2−20 ps time domain, but the dynamics associated with the τ_2 and τ_3 time constants exhibit positive feedback with respect to the time-dependent evolution of **DA** electronic and topological structure. As the mean interporphyryl dihedral angle decreases, further solvent dipolar reorientation occurs, increasing the polarization of the S_1 state, which in turn makes possible augmented diminution of the interporphyryl torsional angle and an even larger excited-state electronic polarization energetically favorable. It is worth noting that many

(51) Birks, J. B. *Photophysics of Aromatic Molecules*; Wiley-Interscience: New York, 1970.
(52) Duncan, T. M.; Rubtsov, I. V.; Susumu, K.; Uyeda, H. T.; Therien, M. J. Manuscript in preparation.
(53) Dogariu, A.; Heeger, A. J. *Phys. Rev. B* **2000**, *61*, 16183−16186.
(54) Cerullo, G.; Lanzani, G.; De Silvestri, S.; Egelhaaf, H.-J.; Luer, L.; Oelkrug, D. *Phys. Rev. B* **2000**, *62*, 2429−2436.
(55) Sariciftci, N. S.; Smolowitz, L.; Cao, Y.; Heeger, A. J. *J. Chem. Phys.* **1993**, *98*, 2664−2669.

chromophores are known to undergo excited structural relaxation following photoexcitation that effects changes in emission transition moment direction and strength;[56−59] while it seems likely that these systems[56−59] would also exhibit a similar type of positive feedback with respect to structural and solvational relaxation dynamics, the combination of substantial emission oscillator strength with a large polarizability in **DA** makes such an effect readily discernible for the first time.

These fast **DA** dynamics indicate a substantial time-dependent change of the magnitude of $\Delta\mu_{ge}$ and are consistent with computational studies that indicate that the $S_1 \rightarrow S_0$ transition moment of this species decreases significantly when the interporphyryl dihedral angle is reduced below 30°. These findings underscore a sensitive dihedral angle dependence of the Franck−Condon overlap for the **DA** S_1 and S_0 potential energy surfaces and account for the facts that (i) the Q_x absorption oscillator strengths of the most planar **DA** conformers, in contrast to the case for **DD**, are reduced with respect to conformers featuring larger torsional angles between their respective PZn least-squares planes; (ii) while the oscillator strength of the **DD** NIR $S_1 \rightarrow S_n$ transition increases with the time-dependent increase in PZn−PZn conjugation, the corresponding **DA** transition probability diminishes over the 20 ps time domain; and (iii) whereas the time-dependent contribution of stimulated emission to the transient spectra remains essentially constant for **DD**, excited-state relaxation in **DA** diminishes the time average $S_1 \rightarrow S_0$ transition oscillator strength by nearly a factor of 3 with respect to that manifest by **DD**.

This work shows that the time-dependent coupling of ground- and excited-state potential energy surfaces in highly conjugated multichromophore systems can be modulated and provides additional understanding into how electronic structure modification can be used to alter independently the properties of ground and excited states. Such insights can potentially be exploited to engineer the magnitudes of the polarizabilities, hyperpolarizabilities, as well as the singlet-excited-state and charge-transfer characteristics of highly conjugated multichromophoric materials.

Acknowledgment. This work was supported by the National Institutes of Health. M.J.T. and K.S. thank, respectively, the Camille and Henry Dreyfus Foundation and the Japanese Society for the Promotion of Science for research fellowships.

Supporting Information Available: Details regarding experimental design and data acquisition, as well as additional transient spectral data. This material is available free of charge via the Internet at http://pubs.acs.org.

JA021157P

(56) Goldie, S. N.; Blanchard, G. J. *J. Phys. Chem. A* **1999**, *103*, 999−1006.
(57) Kwok, W. M.; Ma, C.; Phillips, D.; Matousek, P.; Parker, A. W.; Towrie, M. *J. Phys. Chem. A* **2000**, *104*, 4188−4197.
(58) Leonard, J. D.; Gustafson, T. L. *J. Phys. Chem. A* **2001**, *105*, 1724−1730.
(59) Tan, X.; Gustafson, T. L.; Lefumeux, C.; Burdzinski, G.; Buntinx, G.; Poizat, O. *J. Phys. Chem. A* **2002**, *106*, 3593−3598.